Triggering Emission with the Helical Turn in Thiadiazole-Helicenes

Thomas Biet, Kevin Martin, Jihane Hankache, Nora Hellou, Andreas Hauser, Thomas Bürgi, Tal Aharon, Nicolas Vanthuyne, Marco Caricato, Jeanne Crassous, et al.

Triggering the emission by the helical turn in thiadiazole-helicenes

Thomas Biet,[a] Kévin Martin,[a] Jihane Hankache,[b] Nora Hellou,[c] Andreas Hauser,*[b] Thomas Bürgi,[b] Nicolas Vanthuyne,[d] Tal Aharon,[e] Marco Caricato,*[e] Jeanne Crassous,[c] and Narcis Avarvari*[a]

[a] Dr. T. Biet, K. Martin, Dr. N. Avarvari
Université d'Angers, CNRS UMR 6200
Laboratoire MOLTECH-Anjou, 2 bd Lavoisier, 49045 Angers (France)
Fax: (+33)02 41 73 54 05
E-mail: narcis.avarvari@univ-angers.fr

[b] Dr. J. Hankache, Prof. A. Hauser, Prof. T. Bürgi
Department of Physical Chemistry
University of Geneva
30 Quai Ernest Ansermet, CH-1211 Geneva (Switzerland)
E-mail: Andreas.Hauser@unige.ch

[c] N. Hellou, Dr. J. Crassous
Institut des Sciences Chimiques de Rennes, UMR 6226
CNRS- Université de Rennes 1
Campus de Beaulieu, 35042 Rennes Cedex (France)

[d] Dr. N. Vanthuyne
Aix Marseille Univ, CNRS, Centrale Marseille, iSm2, Marseille, France

[e] T. Aharon, Prof. M. Caricato
Department of Chemistry, University of Kansas
1251 Wescoe Hall Drive, Lawrence, Kansas 66045, United States
E-mail: mcaricato@ku.edu

Abstract: Introduction of heterocycles in the helical skeleton of helicenes allows modulation of their redox, chiroptical and photophysical properties. Herein, we describe the straightforward preparation and structural characterization by single crystal X-ray diffraction of thiadiazole-[7]helicene, which has been resolved into (*M*) and (*P*) enantiomers by chiral HPLC, together with its S-shaped double [4]helicene isomer, as well as the smaller congeners thiadiazole-[5]helicene and benzothiadiazole-anthracene. A copper(II) complex with two thiadiazole-[5]helicene ligands has been structurally characterized and it shows the presence of both (*M*) and (*P*) isomers coordinated to the metal centre. The emission properties of the unprecedented heterohelicenes are highly dependent on the helical turn, as the [7]- and [5]helicene are poorly emissive, whereas their isomers, that is, the S-shaped double [4]helicene and thiadiazole-benzanthracene, are luminescent, with quantum efficiencies of 5.4% and 6.5%, respectively. DFT calculations suggest a quenching of the luminescence of enantiopure [7]helicenes through an intersystem crossing mechanism arising from the relaxed excited S1 state.

Keywords: chirality, helicenes, thiadiazoles, chiroptical properties, DFT calculations

Introduction

Heterohelicenes constitute a particularly interesting family of the non-planar conjugated aromatic helical molecules known as helicenes,[1] as they combine the inherent properties of carbohelicenes such as strong optical rotation and circular dichroism (CD),[2] nonlinear optical properties,[3] self-assembly abilities towards supramolecular materials,[4] with the specificity of the heterocycle or the corresponding heteroatom. A large majority of the reports on heterohelicenes concern either the thiahelicenes, where thiophene units replace totally[5] or partially the benzene rings,[6] or azahelicenes containing pyridine rings,[7] together with their metal complexes.[8] However, other heterocyclic units such as carbazole,[9] pyrane,[10] xanthenium,[11] quinacridinium,[12] pyridinium,[13] phenoxazine,[14] phenothiazine,[15] phosphole,[16] dibenzofurane,[17] or the more exotic azaborine[18] and silole[19] have been included relatively recently in helical structures for different functions and properties. The presence of certain heterocycles in the helical skeleton either provides electroactive character, with the possibility to access chiroptical redox switches, or allows the modulation of the luminescence properties. Concerning the former, besides thiahelicenes[5d] and helquats,[13b] examples of electroactive helicenes which have been studied for the redox modulation of the CD signal are still rare in the literature[20] and include organometallic derivatives of [6]helicene,[21] tetrathiafulvalene-helicenes[22] and helicene-quinones.[23] Note that for a phenothiazine based double hetero[4]helicene a crystalline radical cation salt has been isolated and structurally characterized.[15] On the other hand, it is known that fluorescence quantum yields of carbohelicenes are generally very low due to a very efficient intersystem crossing (ISC) from singlet to triplet excited states,[24] yet the presence of heterocycles such as carbazoles[9] and siloles,[19] possessing themselves luminescent properties, strongly enhances the fluorescence emission of the corresponding heterohelicenes. Moreover, when thiahelicenes are fused with electron acceptor quinoxaline units,[6e] or upon oxidation of the sulfur atoms into sulfones,[25] high fluorescence quantum yields and circularly polarized luminescence are observed, as a consequence of an increased energy gap between the lowest singlet and triplet states. Interesting to note also is the stronger emission for an S-shaped double azahelicene when compared to the simple azahelicene congener.[7d]

A particularly interesting heterocyclic unit for its emission properties and electron-acceptor character is benzothiadiazole (BTD),[26] which has been extensively used during the last decade in the design of materials for red light emission,[27] organic field-effect transistors (OFETs),[28] and photovoltaics,[29] or associated in donor-acceptor dyads with tunable

luminescence.[30] However, thiadiazole units have been never fused to helicene scaffolds to the best of our knowledge. We describe herein the synthesis and the structural characterization of enantiopure thiadiazole-[7]helicene and its S-shaped double [4]helicene, together with the smaller congeners thiadiazole-[5]helicene and thiadiazole-benzanthracene, respectively, as first representatives of a new family of electron poor heterohelicenes. Their chiroptical and photophysical properties, supported by DFT calculations, are investigated. The coordinating character of these helical ligands is highlighted through the preparation and solid state structure of a copper (II) complex containing two thiadiazole-[5]helicene units.

Results and Discussion

Synthesis and solid state structural analysis

The synthesis of the thiadiazole-[7]helicene **1** and double [4]helicene **2** starts with the Wittig reaction between the *in situ* generated phosphorous ylide derived from the phosphonium salt **6** and the benzothiadiazole aldehyde **8**, followed by the oxidative photocyclization[1] of the intermediate stilbene **9** obtained as mixture of *cis* and *trans* isomers (Scheme 1).[31] Thiadiazole-[5]helicene **3** and thiadiazole-benzanthracene **4** have been prepared through a similar strategy, starting from the methyl-naphthalene phosphonium bromide **7** and the same aldehyde **8** as before.

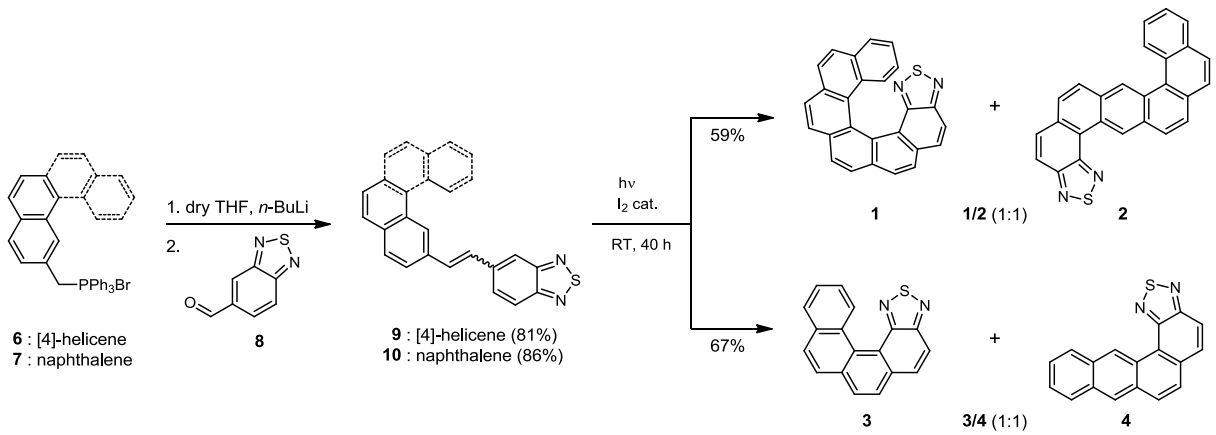

Scheme 1. Synthesis of thiadiazole-helicenes **1**-**4**.

Although the photocyclization reaction is usually highly regioselective with respect to both aromatic units connected *via* the double bond,[1] in the present case we observed selectivity only for the benzothiadiazole moiety, while both possible isomers are formed for the carbocyclic parts, i.e. [4]helicene and naphthalene. They correspond to cyclization at either 1,2- or 2,3-positions, affording, respectively, the hetero-[7]helicene **1** and the fused bis-

[4]helicene **2**, or hetero-[5]helicene **3** and the thiadiazole-benzanthracene **4** which were separated by column chromatography. Note that the same regioselectivity issue for the photocyclization was observed for the formation of [7]carbohelicene *versus* its S-shaped isomer.[32] Since generally [4]helicenes display no particular steric hindrance and have very low racemization barriers,[33] only compound **1** was resolved into its *M* and *P* enantiomers by chiral HPLC, which afforded very good separation.[31] Additionally, attempts to resolve the [5]helicene **3** in the same conditions failed, which is not unexpected as [5]helicene has a racemization barrier of around 24 kcal mol^{-1},[34] confirmed by theoretical calculations,[33,35] and, moreover, replacement of benzene rings by five member ring heterocycles severely reduces this value.[36] The first eluted enantiomer for **1** (using a Chiralpak IF column, see SI for the conditions) was the dextrorotatory, with a specific optical rotation of $[\alpha]_D^{25}$ = +5850±1%° (molar optical rotation $[\phi]_D^{25}$= +22581±1% °cm^2/dmol), corresponding to the clockwise (*P*)-**1** enantiomer, according to the single crystal X-ray analysis (*vide infra*). Note that these values for specific optical and molar optical rotations are of the same order of magnitude as those for the pure [7]carbohelicene, i.e., $[\alpha]_D^{25}$ = +6200±3%° and $[\phi]_D^{25}$= +23465±3% °cm^2/dmol.[37]

Although in the case of helicenes the *P* enantiomer is dextrorotatory,[37b,38] we could also confirm the absolute configuration for the two enantiomers of **1** by single crystal X-ray analysis. Both (*M*)-**1** and (*P*)-**1** crystallize in the orthorhombic chiral space group $P2_12_12_1$, with one independent helicene molecule in general position in the asymmetric unit (Figure 1).

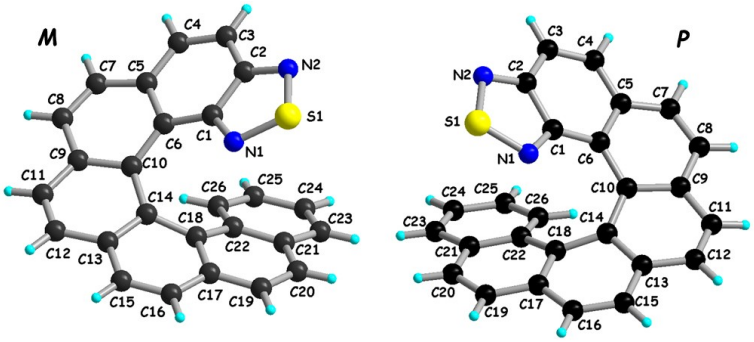

Figure 1. Molecular structures of enantiomeric (*M*)-**1** (left) and (*P*)-**1** (right) together with atom numbering scheme.

The dihedral angle between the terminal rings of the helicene skeleton, defining the helical curvature (hc), amounts to 45°, a typical value for [7]helicenes.[39] The thiadiazole ring overlaps with the terminal benzene C21–C26 with a distance of 3.87 Å between the centroids

of the two cycles and several short N1···C distances, e.g. N1···C22 2.90 Å and N1···C21 3.39 Å, but also partially with the penultimate benzene C17–C22 as shown by the short N1···C18 distance of 2.79 Å (see also Figure S4 and Tables S1-S2). The packing is governed by π-π interactions, with some relatively short intermolecular S···C distances (Figure S5).[31]

The double helicene **2** crystallized in the orthorhombic centrosymmetric space group *P*bca with one independent molecule in the asymmetric unit. The most peculiar structural feature of **2** consists in the almost planarity of the thiadiazole-4[helicene] fragment as indicated by the value of the corresponding dihedral angle of only 8.28°, while the carbo-[4]helicene part shows a twist of 29.13° (Figure 2a and Table S3).

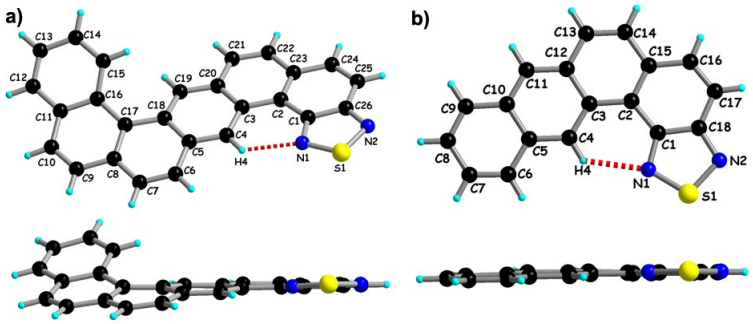

Figure 2. a) Molecular structure of the S-shaped double [4]helicene **2** with an emphasis on the N1···H4 interaction (top) and on the helical twist (bottom); b) Molecular structure of the thiadiazole-benzanthracene **4** with an emphasis on the N1···H4 interaction (top) and side view (bottom).

Interestingly, the intramolecular N1···H4 distance is 2.28 Å, suggesting the establishment of a hydrogen bonding interaction, which may be at the origin of the quasi-planarity of this part of the molecule. Moreover, a similar interaction is likely to occur also in the stilbene type intermediate *cis*-**9** (Scheme 1), stabilizing the conformer providing **2** by cyclization, with respect to the one giving the [7]helicene **1**. This could possibly partially explain the regioselectivity of the photocyclization reaction affording both compounds **1** and **2**, besides the steric hindrance which is also a factor to be taken into account. In the packing of **2** a "segregation" between the carbocyclic part of the molecule and the thiadiazole ring is observed, with establishment of π-π interactions and short intermolecular S···N contacts (Figure S6). Suitable single crystals for X-ray analysis have been obtained as well for the thiadiazole-benzanthracene **4**, having the same thiadiazole-4[helicene] pattern as **2**. It crystallized in the monoclinic system, centrosymmetric space group $P2_1/n$, with one independent molecule in the asymmetric unit. Here again the intramolecular hydrogen bond N1···H4 (2.27 Å) certainly contribute to the planarity of the molecule, with a dihedral angle of only 3.77° between the thiadiazole ring and the C5–C10 benzene ring (Figure 2b and Table

S4). The packing is governed by short intermolecular N···S distances of 3.28 Å providing dyads of **4** through formation of N2S2 rings, as often observed in solid state structures of thiadiazole derivatives,[30a,40] together with aromatic π-π and CH-π interactions (Figure S7).

We have further preliminary estimated the coordinating ability of the thiadiazole-[5]helicene **3** towards Cu(II), as a few examples of benzothiadiazole-Cu(II) complexes have been described in the literature.[41] In thiadiazole-helicenes only the nitrogen atom outside the helical curvature is in principle available for coordination, thus precluding the formation of coordination polymers. Reaction of **3** with the precursors $[Cu(hfac)_2]\cdot xH_2O$ (hfac = hexafluoro-acetylacetonate) in classical conditions[42] provides the complex $Cu(hfac)_2(\mathbf{3})_2$ **5** isolated as pale yellow-green crystals (Scheme 2).

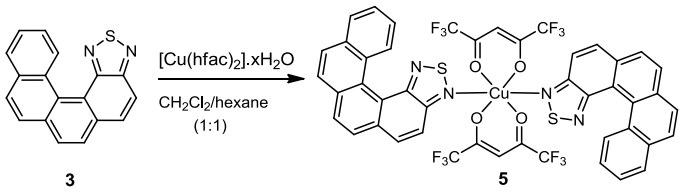

Scheme 2. Synthesis of $Cu(hfac)_2(\mathbf{3})_2$ complex **5**.

The Cu(II) ion is surrounded by four oxygen atoms of the two hfac ligands at Cu–O distances of 1.930 - 1.979 Å and two nitrogen atoms N1 and N3 of thiadiazole ligands disposed in *trans*, with Cu–N bond lengths of 2.42 and 2.49 Å (Table S5), forming an axially distorted octahedral coordination sphere (Figure 3 and S8).

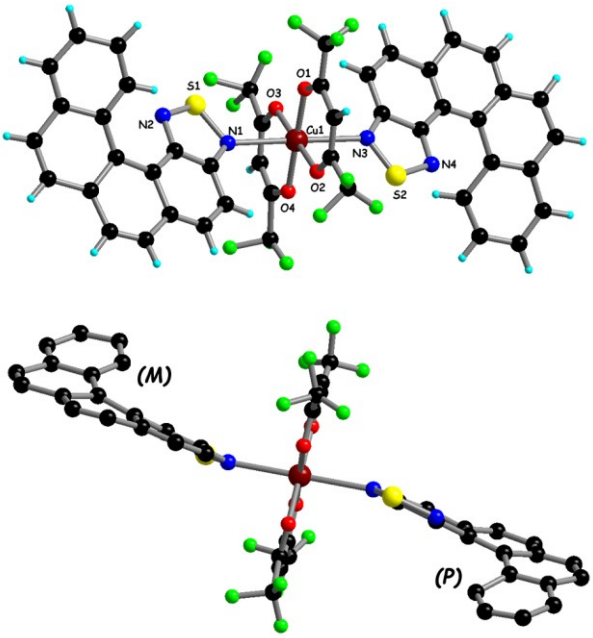

Figure 3. Molecular structure of complex **5** with a partial numbering scheme (top) and a side view showing the two helicities of the ligand (bottom).

The two thiadiazole-[5]helicene ligands show opposite helicities, with helical curvatures of around 40°.

The presence of the thiadiazole ring conferring electron accepting properties, the reduction potentials of the new helical compounds have been determined by cyclic voltammetry measurements. The reduction processes are reversible, with values of -1.53 – -1.54 V *vs* SCE for **1** and **3**, and -1.39 V *vs* SCE for **2** and **4**, respectively (Figure S9 and Table S6).[31]

Chiroptical properties of thiadiazole-[7]helicene 1

As [7]carbohelicenes show strong VCD activity thanks to their rigid helical structure,[43] we have set out to determine VCD spectra for both enantiomers of **1** and compare them with theoretical data. Significant VCD signals are observed between 1000 and 1600 cm^{-1} (Figure 4, see also Figures S10 for IR spectra and S11 for the optimized geometry of (*P*)-**1**), comparable with those in the spectra of [7]helicene. Particularly the bands between 1500 and 1600 cm^{-1}, associated with ring deformation modes, have the same sign in the spectra of **1** and [7]helicene (positive for *M* and negative for *P* enantiomer). Furthermore, all the bands in the range between 1100 and 1300 cm^{-1} have the same sign (negative for *P* enantiomer) both for **1** and [7]helicene. These modes are largely associated with C–H bending modes in the aromatic ring plane. The most prominent band of opposite sign around 1350 cm^{-1} (positive for P enantiomer) is associated with C–C stretching vibrations radial to the helical axis coupled with C–H bending modes in the aromatic ring plane. The antisymmetric N–S stretching vibration of **1** has about one order of magnitude stronger VCD signal than the bands shown in Figure 4, according to the calculations. However, this band arises below 850 cm^{-1} and is therefore not accessible to our VCD measurements. The calculated VCD for the optimized (*P*)-**1** matches very well the experimental curve for the dextrorotatory enantiomer, thus confirming once again the assignment done by single crystal X-ray analysis.

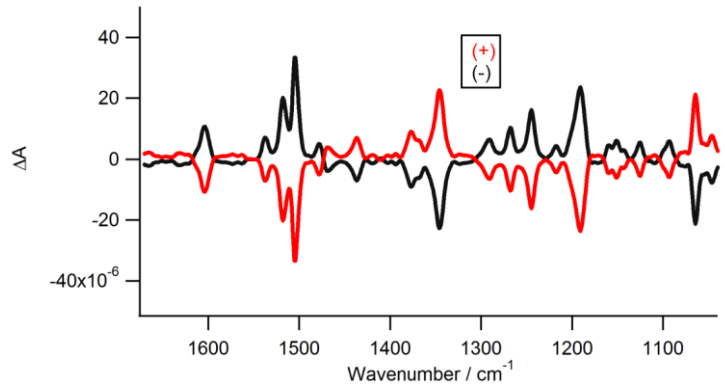

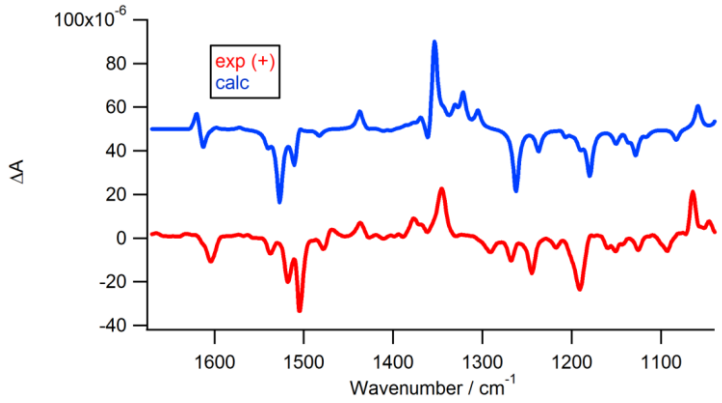

Figure 4. VCD spectra of the two enantiomers of thiadiazole-[7]helicene **1** for solutions of 5 mg in 200 µl CD_2Cl_2 (path length: 0.2 mm, 14000 scans accumulation, a VCD spectrum of the solvent was subtracted) (top). Comparison between the experimental and theoretical VCD spectra for (*P*)-**1** (bottom).

ECD measurements for the two enantiomers (*P*)-(+) and (*M*)-(–) of **1** show the expected object mirror-image relationship, with a series of positive bands at 444, 370, 323 nm and two negative bands at 297 and 241 nm for (*P*)-**1**, while the opposite is observed for (*M*)-**1** (Figure 5 top, including the corresponding experimental absorption spectrum). The UV-vis absorption spectra (see also Figures S12-13) show, as in the case of the ECD, the series of high energy bands, with the most intense one centered at 260 nm, very likely arising from a helicene based π-π* transition,[22] and then at 300 nm and 360 nm. In the lower energy region the weak band appearing at 445 nm (ε = 1300 M^{-1} cm^{-1}) corresponds to an intramolecular charge transfer (ICT) transition from helicene to the thiadiazole acceptor unit (*vide infra*). The calculated ECD and absorption spectra (Figure 5 bottom) excellently reproduce the experimental spectra of (*P*)-**1**, although peak maxima appear blue shifted by about 40 nm. All bands are π→π* excitations that involve different orbitals. The 444 nm band is a HOMO→LUMO charge transfer transition from the helicene structure to the thiadiazole unit. The 370 nm band is also a charge transfer transition from the helicene to the thiadiazole, which can be primarily described as HOMO-2→LUMO and HOMO-1→LUMO+1. The band at 323 nm is primarily a HOMO→LUMO+3 transition, and finally, the negative band at 297 is a transition from the thiadiazole to the helicene backbone (predominantly HOMO-2→LUMO+1 and HOMO-1→LUMO+2). All calculations were performed with the GAUSSIAN suite of programs.[44]

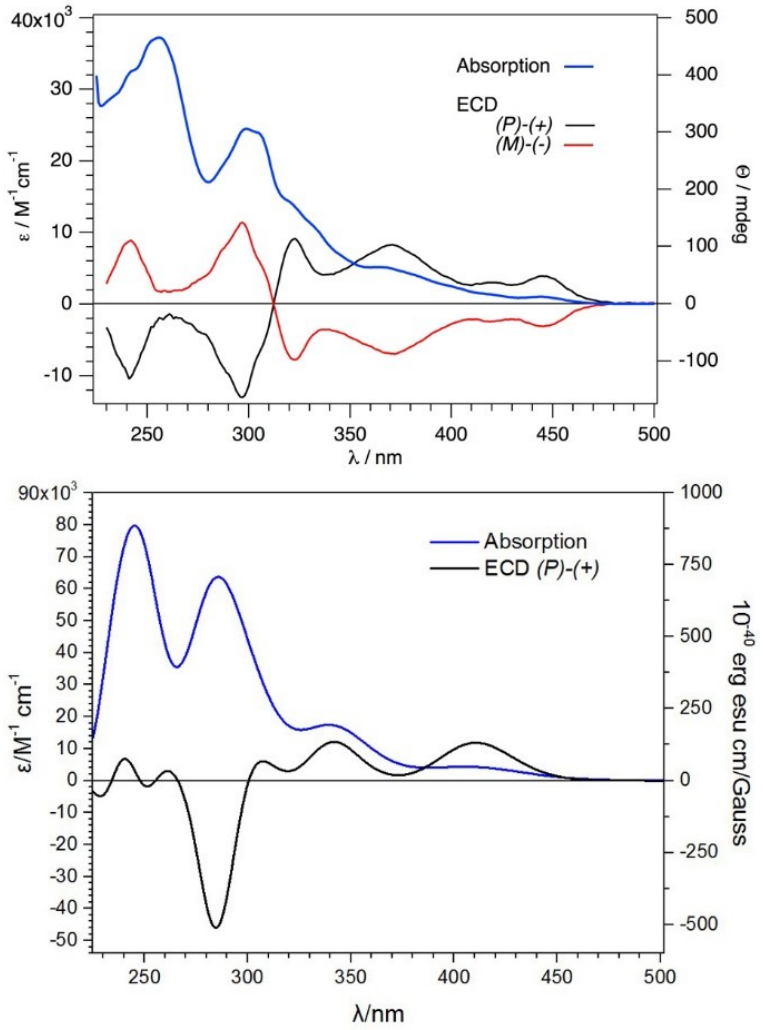

Figure 5. Experimental UV-vis and ECD spectra of **1** in DCM (5×10^{-5} M) at room temperature (top) and theoretical UV-vis and ECD spectra of (*P*)-**1** (bottom); DFT/CAM-B3LYP[45]/aug-cc-pVDZ, solvent: CH_2Cl_2, solvation model: PCM[46] with SMD radii.[47] Excitations appear at 410.67 nm, 342.84 nm, 301.5 nm, 285.19 nm, 262.54 nm, and 243.2 nm.

Interestingly, in the present case the ICT could be operative either through bond, as the molecule is conjugated, or through space thanks to the intramolecular π stacking interaction between thiadiazole and the two terminal benzene units, as suggested by the solid state structure (see Figure 1). This hypothesis is supported by the composition of the frontier orbitals, with the HOMO especially developed on the three terminal benzene rings while the LUMO is concentrated on the BTD part (Figure 6). All of the orbitals and their respective energies are reported in Figure S14 and Table S7 of the supporting information.

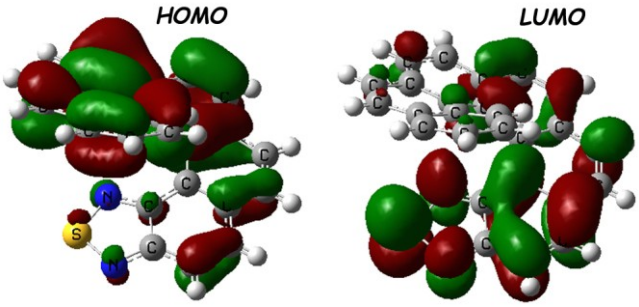

Figure 6. HOMO (-6.85 eV) and LUMO (-1.47 eV) orbitals for (*P*)-**1** (DFT/CAM-B3LYP/aug-cc-pVDZ).

Photophysical properties and theoretical investigations of 1-4

Since the benzothiadiazole (BTD) unit was introduced into the structures of **1-4** for its luminescence, beside the electron poor character, we have set out to determine the emission properties of the helical thiadiazoles. However, as already mentioned, the luminescence of helicenes can be strongly decreased by an intersystem crossing (ISC) mechanism. Upon excitation at λ_{ex} = 365 nm both enantiomers of **1** show a weak emission band centered at 490 nm (20400 cm^{-1}) as shown in Figures S12 for (*M*)-**1** and S13 for (*P*)-**1**. The corresponding excitation spectra do show the main features of the absorption spectra but they are not totally superimposable, probably indicating some underlying impurity luminescence. Thus the experimental quantum yield of < 0.1% is to be regarded as upper limit for the luminescence of compound **1**, which is evidently much lower than the usual values for BTD derivatives.[48] In order to investigate the quenching of the fluorescence, we optimized the geometry of the first excited singlet state of (*P*)-**1**, and we report the energy levels of singlet and triplet states in Figure 7. Assuming that intersystem crossing (ISC) occurs from the relaxed S1 geometry, the plot in Figure 7 shows a favorable energy alignment with nearby triplet states. In order to study the effect of spatial superposition of the terminal rings, we performed similar calculations with smaller congeners both by removing the terminal benzene ring or the thiadiazole ring. The data for these smaller system, reported in the SI (Figures S15-16 and Tables S8-S10) show a worse energy alignment for ISC, in agreement with results for [5]helicene and monoaza[5]helicenes.[49]

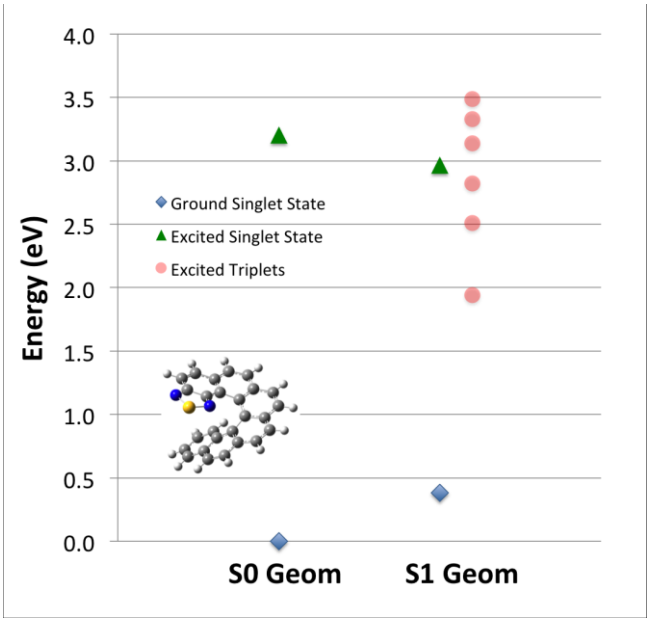

Figure 7. Calculated energy levels (eV) of ground and excited singlet and triplet states for (*P*)-**1**, evaluated at the ground state optimized geometry (S0 Geom) and at the first singlet excited state optimized geometry (S1 Geom). The ground state energy at S0 Geom is used as reference. The energy levels of the triplet states are slightly shifted for clarity. All excited singlet and triplet energy levels are computed with linear response methods.

In striking contrast to **1**, the S-shaped double helicene compound **2** exhibits luminescence in dichloromethane solution both at room temperature, with a broad band centred at 528 nm (Figure 8 top), and a slightly structured band at 77 K (Figure S17), with relatively high emission quantum yield of 5.4% at room temperature when excited at λ_{ex} = 420 nm. The corresponding excitation spectrum is perfectly superimposed with the absorption spectrum, indicating that the luminescence is indeed exclusively from compound **2**.

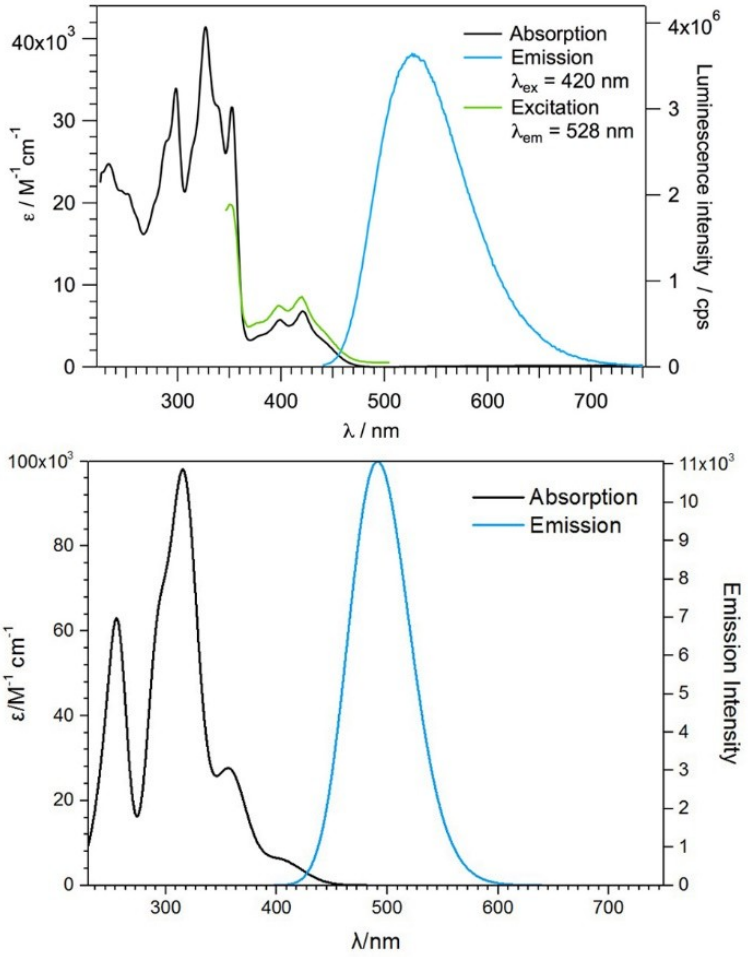

Figure 8. Absorption, emission and excitation spectra of **2** (c = 2.58×10^{-5} M in CH_2Cl_2 solution) at RT; for emission λ_{ex}= 420 nm, for excitation λ_{em}= 528 nm (top). Calculated absorption and emission spectra of **2**; DFT/CAM-B3LYP/aug-cc-pVDZ, solvent: CH_2Cl_2, solvation model: PCM with SMD radii and nonequilibrium solvation; absorption peaks at 316.1 nm, 357.7 nm, and 404.7 nm with a λ_{em} of 491.3 nm (bottom).

The ground state and also the lowest excited state of **2** have been optimized (Figure S18). The calculated absorption and emission spectra reproduce accurately the experimental ones (Figure 8 bottom). From the calculated spectra we are able to assign all of the transitions as primarily $\pi\rightarrow\pi^*$ charge transfer transitions. The absorption peak at 330 nm is due to a transition from the HOMO to the LUMO+2 on the helicene unit (see Figure S19 and Table S11). The lower energy charge transfer transitions are all from the helicene to the thiadiazole unit, differing only in the orbitals involved. The large peak at 360 nm comes primarily from HOMO-1$\rightarrow$LUMO transition, and the broad set of peaks around 400 nm originates from a similar charge transfer between HOMO and LUMO. For the emission spectrum, the calculated peak at λ_{em} = 491.3 nm (corresponding to the experimental peak at λ_{em} = 528 nm)

is characterized by a charge transfer from the LUMO on the thiadiazole unit back to the HOMO on the helicene.

As for **1**, a very weak emission band with maximum at 474 nm was recorded for **3** by excitation in solution at 386 nm (Figure S20). The slight differences of the absorption spectrum with the excitation spectrum (measured at emission wavelength 474 nm) might suggest that this luminescence is probably not real. By cooling the solution at 77 K the luminescence becomes stronger and the spectrum more structured with a slight shift to lower energy (Figure S21). Likewise, the excitation spectrum does not fit perfectly the absorption spectrum, therefore the assignement of this luminescence to some impurity cannot be excluded. Nevertheless, the calculated absorption and emission spectra of **3** are in good agreement with the experimental ones (see Figure S20 and Figure S22 for the optimized geometries of **3** in the ground state and singlet excited state), leaving open the question on the origin of the experimentally observed luminescence.

The photophysical properties of compound **4** resemble those of its longer congener **2**, exhibiting luminescence in dichloromethane solution both at room temperature (Figure 9 top) and at 77 K (Figure S24) with emission quantum yield of 6.5%, slightly higher when compared to **2**. The emission band in solution is centred at 515 nm for an excitation at λ_{ex} = 396 nm. Since the excitation spectra are perfectly superimposed with the absorption spectra, this compound exhibits real luminescence which is further supported by theoretical calculations (Figure 9 bottom and Figure S25 for the optimized geometries of **4** in the ground state and singlet excited state).

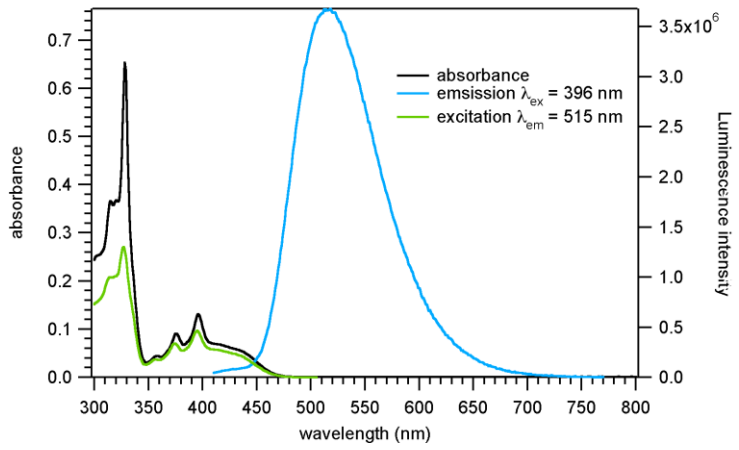

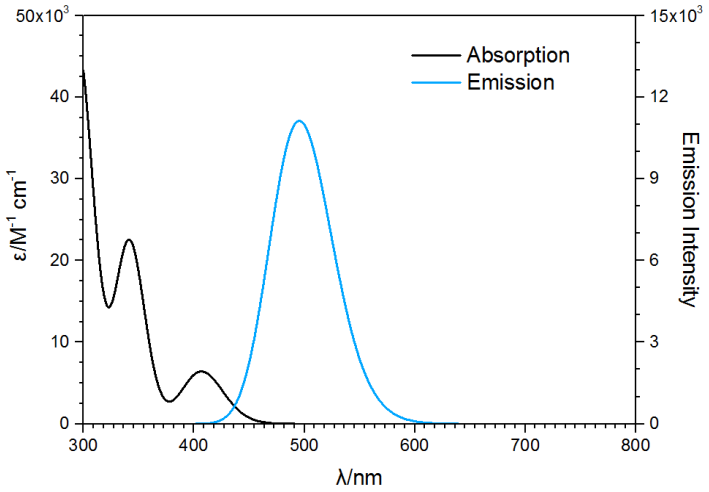

Figure 9. Absorption, emission and excitation spectra of **4** (c = XXX M in CH_2Cl_2 solution) at RT; for emission λ_{ex}= 396 nm, for excitation λ_{em}= 515 nm (top). Calculated absorption and emission spectra of **4**; DFT/CAM-B3LYP/aug-cc-pVDZ, solvent: CH_2Cl_2, solvation model: PCM with SMD radii and nonequilibrium solvation; absorption peaks at 406.7 nm, 341.5 nm and 296 nm with a λ_{em} of 495.2 nm (bottom).

Once again, the agreement between the experimental and calculated spectra allows us to assign the peaks in the absorption and emission spectra. Similar to the longer helicene **2**, the transitions in **4** are primarily $\pi \rightarrow \pi^*$. The peak at 406.7 nm is mainly charge transfer from the HOMO localized on the helicene unit to the LUMO localized on the thiadiazole (see Figure S26). The peak at 341.5 nm is a transition from the HOMO-1, which is more spread out across the entire molecule, to the LUMO. And finally, the peak at 296 nm is a combination of two transitions, both from the HOMO but one to the LUMO+1 and the other to the LUMO+2. The emission peak is a LUMO to HOMO charge transfer from thiadiazole to the helicene unit.

Conclusions

In summary, thiadiazole fused [7]helicene **1** and [5]helicene **3**, together with their S-shaped double [4]helicene **2** and thiadiazole-benzanthracene **4** isomers have been synthesized and structurally characterized. A copper(II) complex (**5**) containing two hfac and two thiadiazole-[5]helicene ligands has been crystallized. The vibrational and electronic chiroptical properties of the enantiomerically pure [7]helicenes have been investigated and supported by theoretical calculations. The photophysical properties of compounds **1**-**4** are highly dependent on the helicity. The DFT calculations accurately reproduced the experimental spectra, allowing the assignment of the transitions between the thiadiazole and helicene units, being mostly of

$\pi \rightarrow \pi^*$ type. In addition, the calculations give a strong rationale for the fluorescence quenching of thiadiazole-[7]helicene **1**, occurring through ISC from the minimum of the S1 state to one of the many triplet states. The shorter [5]helicene **3** is hardly more emissive. In striking contrast, the S-shaped isomer **2** and benzanthracene **4** show strong luminescence. These results open the way towards several directions of investigations such as the use of thiadiazole-helicenes as precursors for other functional helicenes and as ligands for transition metal complexes, the possibility of enhancing the emission properties through oxidation of the sulfur atom in sulfoxide or sulfone and thus observation of CPL,[25] or the exploitation of the electron poor character by association with electron rich moieties into helical donor-acceptors.

Experimental Section

General comments

Dry THF and ether were obtained from a solvent purification system (LC Technology Solutions Incorporated). Nuclear magnetic resonance spectra were recorded on a Bruker Advance DRX 300 spectrometer operating at 300 MHz for ^{1}H and 75 MHz for ^{13}C. Chemical shifts are expressed in parts per million (ppm) downfield from external TMS. The following abbreviations are used: s, singlet; d, doublet; t, triplet; m, multiplet. MALDI-TOF MS spectra were recorded on a Bruker Biflex-IIITM apparatus, equipped with a 337nm N_2 laser. Elemental analyses were recorded using Flash 2000 Fisher Scientific Thermo Electron analyzer. IR spectra were recorded on Bruker FT-IR Vertex 70 spectrometer equipped with a Platinum diamond ATR accessory. UV-Vis absorption spectra for **1** were recorded in solution using either a Lambda 19 or a Lambda 250 PERKIN ELMER spectrometer. Corresponding circular dichroism (CD) measurements were performed with a JASCO Corp. J-715 or J-810 apparatus. UV-Vis absorption spectra for **2** and **4** in CH_2Cl_2 solution were recorded on a Cary 5000 spectrometer. Luminescence and excitation spectra in CH_2Cl_2 solution were recorded on Fluorolog 3 fluorescence spectrophotometer. All luminescence spectra were corrected for the spectral response of the spectrometer and the detector as well as for the irradiation intensity.

5-(2-(benzo[c]phenanthren-2-yl)vinyl)benzo[c][1,2,5]thiadiazole 9: To a suspension of 2-Benzo[c]phenanthrylmethyl-triphenylphosphonium bromide **6** (0.6 g, 1.03 mmol) in dry THF (20 mL) and cooled to -78°C under argon, was added dropwise *n*-butyllithium 1.6 M in hexanes (675 µL, 1.05 eq.) and the resulting solution (orange) was stirred at -78°C for 10 min, warmed to RT over 30 min (turn to red color), then re-cooled to -78°C. A solution of 2,1,3-benzothiadiazole-5-carbaldehyde **8** (169 mg, 1.03 mmol) in THF (5 mL) was then added

dropwise, and the resulting solution (brown/yellow) was stirred at -78°C for 10 min, warmed to RT and stirred for 4 hours. The reaction mixture was filtered over celite and concentrated in vacuo. After chromatography over SiO_2 (CS_2/dichloromethane 2:1 as eluent, Rf = 0.7), **9** was obtained as a yellow solid (*cis*+*trans* mixture) (323 mg, 81%). ^{1}H NMR ($CDCl_3$, 300 MHz) δ (ppm) 9.20 (s, 1H), 9.15 (d, *J* = 8.7 Hz, 1H), 8.07-7.67 (m, 12H), 7.57 (d, *J* = 16.2 Hz, 1H), 7.43 (d, *J* = 16.2 Hz, 1H); Anal. Calc. for $C_{26}H_{16}N_2S$: C, 80.38; H, 4.15; N, 7.21; S, 8.25. Found: C, 80.11; H, 4.02; N, 7.09; S, 8.45%.

5-(2-(naphthalen-2-yl)vinyl)benzo[c][1,2,5]thiadiazole 10: To a suspension of methyl-2-naphthyltriphenylphosphonium bromide (0.7 g, 1.45 mmol) in dry THF (30 mL) and cooled to -78°C under argon, was added dropwise *n*-butyllithium 1.6M in hexanes (0.95 mL, 1.05 eq.) and the resulting solution (orange) was stirred at -78°C for 10 min, warmed to RT over 30 min (turn to red color), then re-cooled to -78°C. A solution of 2,1,3-benzothiadiazole-5-carbaldehyde **8** (238 mg, 1.45 mmol) in THF (5 mL) was then added dropwise, and the resulting solution (brown/yellow) was stirred at -78°C for 10 min, warmed to RT and stirred for 4 hours. The reaction mixture was filtered over celite and concentrated in vacuo. After chromatography over SiO_2 (hexane/dichloromethane 1:1 as eluent, Rf = 0.5), **10** was obtained as a yellow solid (359 mg, 86%). ^{1}H NMR ($CDCl_3$, 300 MHz) δ (ppm) 8.03-7.69 (m, 6H), 7.35-7.56 (m, 4H), 7.00 (d, *J* = 12.2 Hz, $1H_{cis}$), 6.85 (d, *J* = 12.2 Hz, $1H_{cis}$); $\{^1H\}^{13}$C NMR ($CDCl_3$, 75 MHz) δ (ppm); Anal. Calc. for $C_{18}H_{12}N_2S$: C, 74.97; H, 4.19; N, 9.71; S, 11.12. Found: C, 74.71; H, 4.24; N, 9.59; S, 11.43%.

(*rac*)-phenanthro[4',3':5,6]phenanthro[3,4-c][1,2,5]thiadiazole (thiadiazole-[7]helicene) 1 and naphtho[1',2':8,9]tetrapheno[1,2-c][1,2,5]thiadiazole 2: 5-(2-(benzo[c]phenanthren-2-yl)vinyl)benzo[c][1,2,5]thiadiazole **9** (*cis*+*trans* mixture), (300 mg, 0.77 mmol) and iodine (catalytic amount) were dissolved in toluene (700 mL) and placed in a photoreactor equipped with an immersion lamp (150 W). The mixture was irradiated for 40 hours. After evaporation of the solvent and a flash chromatography over SiO_2 (dichloromethane as eluent), a mixture of the two regioisomers **1** and **2** (1:1) was obtained as a yellow solid (176 mg, 59%). A chromatography over SiO_2 (CS_2 as eluent) allowed to separate the two isomers, both as a yellow solid.

1: ^{1}H NMR ($CDCl_3$, 300 MHz) δ (ppm) 8.21 (d, *J* = 8.3 Hz, 1H), 8.16-7.93 (m, 7H), 7.77 (d, *J* = 8.5 Hz, 1H), 7.70 (d, *J* = 9.1 Hz, 1H), 7.54-7.46 (m, 2H), 7.02 (t, *J* = 7.4 Hz, 1H), 6.55 (t, *J* = 7.7 Hz, 1H); $\{^1H\}^{13}$C NMR ($CDCl_3$, 75 MHz) δ (ppm) 153.8, 152.3, 133.2, 132.3, 132.1, 132.0, 131.9, 130.5, 129.91, 129.86, 129.3, 128.4, 128.3, 127.2, 127.1, 127.0, 126.8, 126.4, 126.2, 126.0, 125.6, 124.8, 124.5, 124.3, 123.6, 119.5; MS (MALDI-TOF) m/z = 386 (M^+),

calcd. 386.09; Anal. Calc. for $C_{26}H_{14}N_2S$: C, 80.80; H, 3.65; N, 7.25; S, 8.30. Found: C, 80.64; H, 3.58; N, 7.15; S, 8.58%.

2: ^{1}H NMR ($CDCl_3$, 300 MHz) δ (ppm) 11.10 (s, 1H), 9.82 (s, 1H), 9.39 (d, *J* = 8.6 Hz, 1H), 8.39 (d, *J* = 8.7 Hz, 1H), 8.35 (d, *J* = 8.8 Hz, 1H), 8.21-7.90 (m, 7H), 7.83 (t, *J* = 7.7 Hz, 1H), 7.77-7.69 (m, 1H); {^{1}H}^{13}C NMR ($CDCl_3$, 75 MHz) δ (ppm) 155.4, 153.8, 133.63, 133.62, 132.93, 132.87, 131.3, 131.0, 129.0, 128.9, 128.8, 128.3, 128.2, 128.0, 128.8, 127.8, 127.6, 127.5, 128.2, 126.9, 126.7, 126.4, 125.9, 120.3; MS (MALDI-TOF) m/z = 386 (M^+), calcd. 386.09; Anal. Calc. for $C_{26}H_{14}N_2S$: C, 80.80; H, 3.65; N, 7.25; S, 8.30. Found: C, 80.62; H, 3.58; N, 7.15; S, 8.52%.

benzo[5,6]phenanthro[3,4-c][1,2,5]thiadiazole (thiadiazole-[5]helicene) 3 and tetrapheno[1,2-c][1,2,5]thiadiazole 4: 5-(2-(naphthalen-2-yl)vinyl)benzo[c][1,2,5]thiadiazole **10** (*cis*+*trans* mixture), (300 mg, 1.04 mmol) and iodine (catalytic amount) were dissolved in toluene (700 mL) and placed in a photoreactor equipped with an immersion lamp (150 W). The mixture was irradiated for 40 hours. After evaporation of the solvent and a flash chromatography over SiO_2 (dichloromethane as eluent), a mixture of the two isomers, **3/4** (1:1) was obtained as a yellow solid (200 mg, 67%). A chromatography over SiO_2 (CS_2 as eluent) allowed to separate the two isomers, both as yellow solids.

3 ^{1}H NMR ($CDCl_3$, 300 MHz) δ (ppm) 11.50 (d, *J* = 8.3 Hz, 1H), 8.56-7.88 (m, 6H), 8.27 (s, 1H), 7.55 (d, *J* = 8.6 Hz, 1H), 6.92 (t, *J* = 8.0 Hz, 1H), 6.15 (t, *J* = 8.4 Hz, 1H); {^{1}H}^{13}C NMR ($CDCl_3$, 75 MHz) δ (ppm) 155.0, 153.6, 133.8, 133.4, 133.0, 132.9, 129.74, 129.69, 129.67, 129.0, 128.4, 127.54, 127.49, 127.20, 126.0, 123.9, 123.1, 119.8; Anal. Calc. for $C_{18}H_{10}N_2S$: C, 75.50; H, 3.52; N, 9.78; S, 11.20. Found: C, 75.28; H, 3.59; N, 9.57; S, 11.41%.

4 ^{1}H NMR ($CDCl_3$, 300 MHz) δ (ppm) 11.08 (s, 1H), 8.56 (s, 1H), 8.40-8.32 (m, 1H), 8.20 (d, *J* = 8.8 Hz, 1H), 8.15-8.10 (m, 2H), 8.05 (d, *J* = 9.0 Hz, 1H), 7.84 (d, *J* = 8.8 Hz, 1H), 7.69-7.60 (m, 2H); {^{1}H}^{13}C NMR ($CDCl_3$, 75 MHz) δ (ppm) 155.4, 153.8, 133.3, 132.9, 132.8, 131.8, 131.2, 131.0, 129.5, 128.2, 127.8, 127.0, 126.5, 126.3, 126.0, 119.8; Anal. Calc. for $C_{18}H_{10}N_2S$: C, 75.50; H, 3.52; N, 9.78; S, 11.20. Found: C, 75.62; H, 3.61; N, 9.58; S, 11.08%.

Complex 5: In a Schlenk tube **3** (12 mg, 0.042 mmol) and $[Cu(hfac)_2]\cdot xH_2O$ (10 mg, 0.021 mmol) were stirred at 60 °C in a 8 mL mixture hexane/dichloromethane (1:1) during 1h. Then, the solution was allowed to return to room temperature, and pale yellow/green crystals of **5** were obtained after slow evaporation of solvents (20 mg, 90%). Anal. Calc. for $C_{46}H_{22}CuF_{12}N_4O_4S_2$: C, 52.60; H, 2.11; N, 5.33; S, 6.11. Found: C, 52.45; H, 2.18; N, 5.25; S, 6.32%.

X-Ray structure determinations: Details about data collection and solution refinement are given in Table 1. X-ray diffraction measurements were performed on a Bruker Kappa CCD diffractometer, operating with a $Mo_{K\alpha}$ (λ=0.71073 Å) X-ray tube with a graphite monochromator. The structures were solved (SHELXS-97) by direct methods and refined (SHELXL-97) by full matrix least-square procedures on F^2.[50] All non-hydrogen atoms were refined anisotropically. Hydrogen atoms were introduced at calculated positions (riding model), included in structure factor calculations but not refined. Crystallographic data for the five structures have been deposited with the Cambridge Crystallographic Data Centre, deposition numbers CCDC 1487949 ((*M*)-**1**), 1487950 ((*P*)-**1**), 1487951 (**2**), 1500339 (**4**) and 1500340 (**5**). These data can be obtained free of charge from CCDC, 12 Union road, Cambridge CB2 1EZ, UK (e-mail: deposit@ccdc.cam.ac.uk or http://www.ccdc.cam.ac.uk).

Table 1. Crystal Data and Structure Refinement for (*M*)-**1**, (*P*)-**1**, **2**, **4** and **5**.

Compound	(*M*)-**1**	(*P*)-**1**	**2**	**4**	**5**
empirical formula	$C_{26}H_{14}N_2S$	$C_{26}H_{14}N_2S$	$C_{26}H_{14}N_2S$	$C_{18}H_{10}N_2S$	$C_{46}H_{22}CuF_{12}N_4O_4S_2$
fw	386.45	386.45	386.45	286.34	1050.34
T (K)	293(2)	293(2)	293(2)	293(2)	293(2)
wavelength (Å)	0.71073	0.71073	0.71073	0.71073	0.71073
cryst syst	Orthorhombic	Orthorhombic	Orthorhombic	Monoclinic	Monoclinic
space group	$P2_12_12_1$	$P2_12_12_1$	*P*bca	$P2_1/n$	*C*c
a (Å)	8.4500 (9)	8.4492 (7)	8.8179 (7)	13.7510 (9)	27.195 (2)
b (Å)	13.7216 (19)	13.7240 (13)	17.3503 (17)	6.1357 (3)	9.2166 (7)
c (Å)	16.265 (3)	16.2628 (13)	24.0917 (15)	15.8590 (10)	18.863 (9)
α(deg)	90.00	90.00	90.00	90.00	90.00
β(deg)	90.00	90.00	90.00	99.759 (6)	111.230 (4)
γ(deg)	90.0	90.0	90.0	90	90.0
V (Å^3)	1885.9 (4)	1885.8 (3)	3685.9 (5)	1318.69 (14)	4407.1 (5)
Z	4	4	8	4	4
D_c (g cm^{-3})	1.361	1.361	1.393	1.442	1.583
abs coeff (mm^{-1})	0.186	0.186	0.191	0.238	0.691
Flack parameter	0.11(16)	0.12(19)			
GOF on F^2	1.049	1.089	1.026	1.085	1.048
final *R* indices [$I > 2\sigma(I)$]	R1 = 0.0707, wR2 = 0.1567	R1 = 0.0676, wR2 = 0.1304	R1 = 0.0456, wR2 = 0.0987	R1 = 0.0485, wR2 = 0.1206	R1 = 0.0560, wR2 = 0.0986
R indices (all data)	R1 = 0.1485 wR2 = 0.1867	R1 = 0.1236 wR2 = 0.1523	R1 = 0.0937 wR2 = 0.1157	R1 = 0.0891, wR2 = 0.1364	R1 = 0.1562 wR2 = 0.1313

[a] $R(F_o) = \Sigma||F_o| - |F_c||/\Sigma|F_o|$; $R_w(F_o^2) = [\Sigma[w(F_o^2 - F_c^2)^2]/\Sigma[w(F_o^2)^2]]^{1/2}$

Acknowledgements

This work was supported in France by the CNRS through the GDR 3712 Chirafun, the University of Angers and the French Ministry of Education and Research (grant to T.B.). The investigation was supported in part by the University of Kansas General Research Fund allocation #2302049, by the University of Kansas startup fund (T.A. and M.C.), the University of Geneva and by the Swiss National Science foundation (grant No

200020_152780). J.C. and N.A. warmly thank Chengshuo Shen (University of Rennes 1) and Flavia Pop (University of Angers) for technical help.

References

[1] a) R. H. Martin, *Angew. Chem. Int. Ed. Engl.* **1974**, *13*, 649–660; b) Y. Shen, C.-F. Chen, *Chem. Rev.* **2012**, *112*, 1463–1535; c) M. Gingras, *Chem. Soc. Rev.* **2013**, *42*, 968–1006.

[2] a) F. Furche, R. Ahlrichs, C. Wachsmann, E. Weber, A. Sobanski, F. Vogtle, S. Grimme, *J. Am. Chem. Soc.* **2000**, *122*, 1717–1724; b) J. Autschbach, *Chirality* **2010**, *22*, E116–E152; c) M. Gingras, G. Félix, R. Peresutti, *Chem. Soc. Rev.* **2013**, *42*, 1007–1050.

[3] a) T. Verbiest, S. Van Elshocht, M. Kauranen, L. Hellemans, J. Snauwaert, C. Nuckolls, T. J. Katz, A. Persoons, *Science* **1998**, *282*, 913–915; b) A. Bossi, E. Licandro, S. Maiorana, C. Rigamonti, S. Righetto, G. R. Stephenson, M. Spassova, E. Botek, B. Champagne, *J. Phys. Chem. C* **2008**, *112*, 7900–7907.

[4] a) C. Nuckolls, T. J. Katz, L. Castellanos, *J. Am. Chem. Soc.* **1996,** *118,* 3767–3768; b) M. Gingras, *Chem. Soc. Rev.* **2013**, *42*, 1051–1095.

[5] a) A. Rajca, M. Miyasaka, M. Pink, H. Wang, S. Rajca, *J. Am. Chem. Soc.* **2004**, *126*, 15211–15222; b) M. Miyasaka, M. Pink, S. Rajca, A. Rajca, *Angew. Chem. Int. Ed.* **2009**, *48*, 5954–5957; c) C. Li, J. Shi, L. Xu, Y. Wang, Y. Cheng, H. Wang, *J. Org. Chem.* **2009**, *74*, 408–411; d) J. K. Zak, M. Miyasaka, S. Rajca, M. Lapkowski, A. Rajca, *J. Am. Chem. Soc.* **2010**, *132*, 3246–3247; e) M. Miyasaka, M. Pink, A. Olankitwanit, S. Rajca, A. Rajca, *Org. Lett.* **2012**, *14*, 3076–3079.

[6] a) T. B. Norsten, A. Peters, R. McDonald, M. Wang, N. R. Branda, *J. Am. Chem. Soc.* **2001,** *123,* 7447–7448; b) A. Rajca, M. Pink, S. Xiao, M. Miyasaka, S. Rajca, K. Das, K. Plessel, *J. Org. Chem.* **2009**, *74*, 7504–7513; c) F. Rose-Munch, M. Li, E. Rose, J. C. Daran, A. Bossi, E. Licandro, P. R. Mussini, *Organometallics* **2012**, *31*, 92−104; d) T. Fujikawa, Y. Segawa, K. Itami, *J. Am. Chem. Soc.* **2016**, *138*, 3587−3595; e) Y. Yamamoto, H. Sakai, J. Yuasa, Y. Araki, T. Wada, T. Sakanoue, T. Takenobu, T. Kawai, T. Hasobe, *Chem. Eur. J.* **2016**, *22*, 4263–4273.

[7] a) J. Míšek, F. Teplý, I. G. Stará, M. Tichý, D. Šaman, I. Císařová, P. Vojtíšek, I. Starý, *Angew. Chem. Int. Ed.* **2008***, 47*, 3188–3191; b) S. Graule, M. Rudolph, N. Vanthuyne, J. Autschbach, C. Roussel, J. Crassous, R. Réau, *J. Am. Chem. Soc.* **2009**, *131*, 3183–

3185; c) A. Ueda, H. Wasa, S. Suzuki, K. Okada, K. Sato, T. Takui, Y. Morita, *Angew. Chem. Int. Ed.* **2012**, *51*, 6691–6695; d) K. Nakamura, S. Furumi, M. Takeuchi, T. Shibuya, K. Tanaka, *J. Am. Chem. Soc.* **2014**, *136*, 5555−5558; e) T. Caronna, A. Mele, A. Famulari, D. Mendola, F. Fontana, M. Juza, M. Kamuf, K. Zawatzky, O. Trapp, *Chem. Eur. J.* **2015**, *21*, 13919–13924.

[8] a) S. Graule, M. Rudolph, W. Shen, J. A. G. Williams, C. Lescop, J. Autschbach, J. Crassous, R. Réau, *Chem. Eur. J.* **2010**, *16*, 5976–6005; b) D. Mendola, N. Saleh, N. Vanthuyne, C. Roussel, L. Toupet, F. Castiglione, T. Caronna, A. Mele, J. Crassous, *Angew. Chem. Int. Ed*. **2014**, *53*, 5786–5790; c) D. Mendola, N. Saleh, N. Hellou, N. Vanthuyne, C. Roussel, L. Toupet, F. Castiglione, F. Melone, T. Caronna, F. Fontana, J. Martí-Rujas, E. Parisini, L. Malpezzi, A. Mele, J. Crassous, *Inorg. Chem.* **2016**, *55*, 2009−2017.

[9] a) Y. Ooyama, G. Ito, K. Kushimoto, K. Komaguchi, I. Imae, Y. Harimab, *Org. Biomol. Chem.* **2010**, *8*, 2756–2770; b) L. Shi, Z. Liu, G. Dong, L. Duan, Y. Qiu, J. Jia, W. Guo, D. Zhao, D. Cui, X. Tao, *Chem. Eur. J.* **2012**, *18*, 8092–8099; c) K. Goto, R. Yamaguchi, S. Hiroto, H. Ueno, T. Kawai, H. Shinokubo, *Angew. Chem. Int. Ed.* **2012**, *51*, 10333–10336.

[10] a) T. Kaseyama, S. Furumi, X. Zhang, K. Tanaka, M. Takeuchi, *Angew. Chem. Int. Ed.* **2011**, *50*, 3684–3687; b) J. Zádný, A. Jančařík, A. Andronova, M. Šámal, J. Vacek Chocholoušová, J. Vacek, R. Pohl, D. Šaman, I. Císařová, I. G. Stará, I. Starý, *Angew. Chem. Int. Ed.* **2012**, *51*, 5857–5861;

[11] J. Guin, C. Besnard, J. Lacour, *Org. Lett.* **2010**, *12,* 1748–1751.

[12] a) C. Herse, D. Bas, F. C. Krebs, T. Bürgi, J. Weber, T. Wesolowski, B. W. Laursen, J. Lacour, *Angew. Chem. Int. Ed.* **2003**, *42*, 3162–3166; b) O. Kel, P. Sherin, N. Mehanna, B. Laleu, J. Lacour, E. Vauthey, *Photochem. Photobiol. Sci.* **2012**, *11*, 623–631.

[13] a) L. Adrianssens, L. Severa, T. Šálová, I. Císařová, R. Pohl, D. Šaman, S. V. Rocha, N. S. Finney, L. Pospíšil, P. Slavíček, F. Teplý, *Chem. Eur. J.* **2009**, *15*, 1072–1076; b) L. Pospíšil, L. Bednárová, P. Štěpánek, P. Slavíček, J. Vávra, M. Hromadová, H. Dlouhá, J. Tarábek, F. Teplý, *J. Am. Chem. Soc.* **2014**, *136*, 10826−10829; c) B. J. Coe, D. Rusanova, V. D. Joshi, S. Sánchez, J. Vávra, D. Khobragade, L. Severa, I. Císařová, D. Šaman, R. Pohl, K. Clays, G. Depotter, B. S. Brunschwig, F. Teplý, *J. Org. Chem.* **2016**, *81*, 1912−1920.

[14] D. Sakamaki, D. Kumano, E. Yashima, S. Seki, *Angew. Chem. Int. Ed.* **2015**, *54*, 5404–5407.

[15] D. Sakamaki, D. Kumano, E. Yashima, S. Seki, *Chem. Commun.* **2015**, *51*, 17237–17240.

[16] a) K. Nakano, H. Oyama, Y. Nishimura, S. Nakasako, K. Nozaki, *Angew. Chem. Int. Ed.* **2012**, *51*, 695–699; b) K. Yavari, S. Moussa, B. Ben Hassine, P. Retailleau, A. Voituriez, A. Marinetti, *Angew. Chem. Int. Ed.* **2012**, *51*, 6748–6752; c) K. Yavari, P. Retailleau, A. Voituriez, A. Marinetti, *Chem. Eur. J.* **2013**, *19*, 9939–9947.

[17] M. S. Sundar, A. V. Bedekar, *Org. Lett.* **2015**, *17*, 5808−5811.

[18] T. Hatakeyama, S. Hashimoto, T. Oba, M. Nakamura, *J. Am. Chem. Soc.* **2012**, *134*, 19600−19603.

[19] H. Oyama, K. Nakano, T. Harada, R. Kuroda, M. Naito, K. Nobusawa, K. Nozaki, *Org. Lett.* **2013**, *15*, 2104–2107.

[20] a) T. J. Katz, A. Sudhakar, M. F. Teasley, A. M. Gilbert, W. E. Geiger, M. P. Robben, M. Wuensch, M. D. Ward, *J. Am. Chem. Soc.* **1993**, *115*, 3182–3198; b) H. Isla, J. Crassous, *C. R. Chimie* **2016**, *19*, 39–49.

[21] a) E. Anger, M. Srebro, N. Vanthuyne, L. Toupet, S. Rigaut, C. Roussel, J. Autschbach, J. Crassous, R. Réau, *J. Am. Chem. Soc.* **2012**, *134*, 15628−15631; b) C. Shen, G. Loas, M. Srebro-Hooper, N. Vanthuyne, L. Toupet, O. Cador, F. Paul, J. T. López Navarrete, F. J. Ramírez, B. Nieto-Ortega, J. Casado, J. Autschbach, M. Vallet, J. Crassous, *Angew. Chem. Int. Ed.* **2016**, *ASAP*, DOI: 10.1002/anie.20160163.

[22] T. Biet, A. Fihey, T. Cauchy, N. Vanthuyne, C. Roussel, J. Crassous, N. Avarvari, *Chem. Eur. J.* **2013**, *19*, 13160–13167.

[23] D. Schweinfurth, M. Zalibera, M. Kathan, C. Shen, M. Mazzolini, N. Trapp, J. Crassous, G. Gescheidt, F. Diederich, *J. Am. Chem. Soc.* **2014**, *136*, 13045−13052.

[24] M. Sapir, E. V. Donckt, *Chem. Phys. Lett.* **1975**, *36*, 108–110.

[25] Y. Yamamoto, H. Sakai, J. Yuasa, Y. Araki, T. Wada, T. Sakanoue, T. Takenobu, T. Kawai, T. Hasobe, *J. Phys. Chem. C* **2016**, *120*, 7421−7427.

[26] a) B. A. D. Neto, A. A. M. Lapis, E. N. da Silva Júnior, J. Dupont, *Eur. J. Org. Chem.* **2013**, 228–255; b) B. A. D. Neto, P. H. P. R. Carvalho, J. R. Correa, *Acc. Chem. Res.* **2015**, *48*, 1560−1569.

[27] a) C. T. Chen, *Chem. Mater.* **2004**, *16*, 4389–4400; b) K. R. J. Thomas, J. T. Lin, M. Velusamy, Y.-T. Tao, C.-H. Chuen, *Adv. Funct. Mater.* **2004**, *14*, 83–90.

[28] a) J. Zaumseil, C. L. Donley, J.-S. Kim, R. H. Friend, H. Sirringhaus, *Adv. Mater.* **2006**, *18*, 2708–2712; b) T. Kono, D. Kumaki, J. Nishida, T. Sakanoue, M. Kakita, H. Tada, S. Tokito, Y. Yamashita, *Chem. Mater.* **2007**, *19*, 1218–1220; c) M. Zhang, H. N. Tsao, W. Pisula, C. Yang, A. K. Mishra, K. Müllen, *J. Am. Chem. Soc.* **2007**, *129*, 3472–3473; d) Y. Yamashita, *Chem. Lett.* **2009**, *38*, 870–875.

[29] a) M. Velusamy, K. R. J. Thomas, J. T. Lin, Y. Hsu, K. Ho, *Org. Lett.* **2005**, *7*, 1899–1902; b) Z.-M. Tang, T. Lei, K.-J. Jiang, Y.-L. Song, J. Pei, *Chem Asian J.* **2010**, *5*, 1911–1917; c) Y. Lin, Y. Li, X. Zhan, *Chem. Soc. Rev.* **2012**, *41*, 4245–4272.

[30] a) F. Pop, A. Amacher, N. Avarvari, J. Ding, L. M. Lawson Daku, A. Hauser, M. Koch, J. Hauser, S.-X. Liu, S. Decurtins, *Chem. Eur. J.* **2013**, *19*, 2504–2514; b) F. Pop, S. Seifert, J. Hankache, J. Ding, A. Hauser, N. Avarvari, *Org. Biomol. Chem.* **2015**, *13*, 1040–1047; c) F. Pop, N. Avarvari, *Chem. Commun.* **2016**, *52*, 7906–7927.

[31] Experimental details and characterization of compounds, X-ray data, CV, UV-vis, ECD, VCD, photophysical measurements and theoretical calculations details are provided in the Supporting Information. CCDC 1487949 ((*M*)-**1**), 1487950 ((*P*)-**1**), 1487951 (**2**), 1500339 (**4**) and 1500340 (**5**) contain the supplementary crystallographic data (cif files) for this paper. These data can be obtained free of charge from The Cambridge Crystallographic Data Centre via www.ccdc.cam.ac.uk/data_request/cif.

[32] H. R. Talele, A. R. Chaudhary, P. R. Patel, A. V. Bedekar, *ARKIVOC* **2011**, 15–37.

[33] S. Grimme, S. D. Peyerimhoff, *Chem. Phys.* **1996***, 204,* 411–417.

[34] C. Goedicke, H. Stegemeyer, *Tetrahedron Lett.* **1970**, 937–940.

[35] R. H. Janke, G. Haufe, E.-U. Würthwein, J. H. Borkent, *J. Am. Chem. Soc.* **1996**, *118,* 6031–6035.

[36] B. Abarca, R. Ballesteros, R. Adam, R. Ballesteros-Garrido, F. R. Leroux, F. Colobert, I. Alkorta, J. Elguero, *Tetrahedron* **2014**, *70*, 8750–8757.

[37] a) R. H. Martin, M. Flammang-Barbieux, J. P. Cosyn, M. Gelbcke, *Tetrahedron Lett.* **1968**, *9*, 3507–3510; b) M. Srebro, N. Govind, W. A. de Jong, J. Autschbach, *J. Phys. Chem. A* **2011**, *115*, 10930–10949.

[38] D. A. Lightner, D. T. Hefelfinger, T. W. Powers, G. W. Frank, K. N. Trueblood, *J. Am. Chem. Soc.* **1972**, *94*, 3492–3497.

[39] a) P. T. Beurskens, G. Beurskens, T. E. M. van den Hark, *Cryst. Struct. Comm.* **1976**, *5*, 241; b) T. E. M. van den Hark, P. T. Beurskens, *Cryst. Struct. Comm.* **1976**, *5*, 247.

[40] A. F. Cozzolino, I. Vargas-Baca, S. Mansour, A. H. Mahmoudkhani, *J. Am. Chem. Soc.* **2005**, *127*, 3184–3190.

[41] a) G. S. Papaefstathiou, A. Tsohos, C. P. Raptopoulou, A. Terzis, V. Psycharis, D. Gatteschi, S. P. Perlepes, *Cryst. Growth Des.* **2001**, *1*, 191–194; b) K. Skorda, G. S. Papaefstathiou, A. Vafiadis, A. Lithoxoidou, C. P. Raptopoulou, A. Terzis, V. Psycharis, E. Bakalbassis, V. Tangoulis, S. P. Perlepes, *Inorg. Chim. Acta* **2001**, *326*, 53–64.

[42] A. M. Madalan, C. Réthoré, N. Avarvari, *Inorg. Chim. Acta* **2007**, *360*, 233–240.

[43] T. Bürgi, A. Urakawa, B. Behzadi, K.-H. Ernst, A. Baiker, *New J. Chem.* **2004**, *28*, 332–334.

[44] M. J. Frisch, G. W. Trucks, H. B. Schlegel, G. E. Scuseria, M. A. Robb, J. R. Cheeseman, G. Scalmani, V. Barone, B. Mennucci, G. A. Petersson, H. Nakatsuji, M. Caricato, X. Li, H. P. Hratchian, A. F. Izmaylov, J. Bloino, G. Zheng, J. L. Sonnenberg, M. Hada, M. Ehara, K. Toyota, R. Fukuda, J. Hasegawa, M. Ishida, T. Nakajima, Y. Honda, O. Kitao, H. Nakai, T. Vreven, J. A. MontgomeryJr., J. E. Peralta, F. Ogliaro, M. Bearpark, J. J. Heyd, E. Brothers, K. N. Kudin, V. N. Staroverov, T. Keith, R. Kobayashi, J. Normand, K. Raghavachari, A. Rendell, J. C. Burant, S. S. Iyengar, J. Tomasi, M. Cossi, N. Rega, J. M. Millam, M. Klene, J. E. Knox, J. B. Cross, V. Bakken, C. Adamo, J. Jaramillo, R. Gomperts, R. E. Stratmann, O. Yazyev, A. J. Austin, R. Cammi, C. Pomelli, J. W. Ochterski, R. L. Martin, K. Morokuma, V. G. Zakrzewski, G. A. Voth, P. Salvador, J. J. Dannenberg, S. Dapprich, P. V. Parandekar, N. J. Mayhall, A. D. Daniels, O. Farkas, J. B. Foresman, J. V. Ortiz, J. Cioslowski, D. J. Fox, Gaussian Development Version, Revision H.09+, Gaussian, Inc., Wallingford, CT, **2010**.

[45] T. Yanai, D. P. Tew, N. C. Handy, *Chem. Phys. Lett.* **2004**, *393*, 51–57.

[46] a) J. Tomasi, B. Mennucci, R. Cammi, *Chem. Rev.* **2005**, *105*, 2999–3093; b) J. Tomasi, B. Mennucci, E. Cancès, *J. Mol. Struct. (Theochem)* **1999**, *464*, 211–226; c) G. Scalmani, M. J. Frisch, *J. Chem. Phys.* **2010**, *132*, 114110.

[47] A. Marenich, C. Cramer, D. Truhlar, *J. Phys. Chem. B* **2009**, *113*, 6378–6396.

[48] J. Pina, J. Seixas de Melo, D. Breusov, U. Scherf, *Phys. Chem. Chem. Phys.* **2013**, *15*, 15204–15213.

[49] K. Schmidt, S. Brovelli, V. Coropceanu, D. Beljonne, J. Cornil, C. Bazzini, T. Caronna,| R. Tubino, F. Meinardi, Z. Shuai, J.-L. Brédas, *J. Phys. Chem. A* **2007**, *111*, 10490–10499.

[50] G. M. Sheldrick, *Programs for the Refinement of Crystal Structures*, University of Göttingen, Göttingen, Germany, **1996**.